

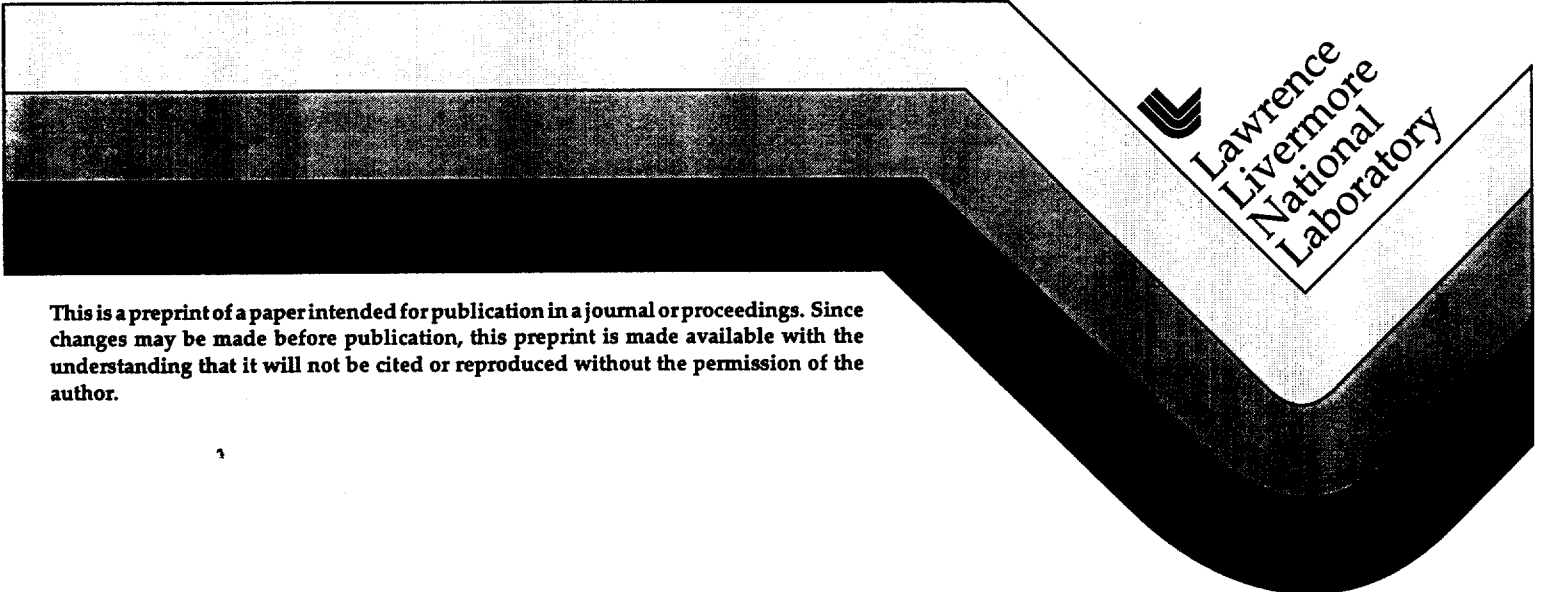
UCRL-JC-129251
PREPRINT

Hot Electron Production and Heating by Hot Electrons in Fast Ignitor Research

M. H. Key, K. Estabrook, B. Hammel, S. Hatchett, D. Hinkel,
J. Kilkenny, J. Koch, W. Kruer, B. Langdon, B. Lasinski, R. Lee,
B. MacGowan, J. Moody, M. Moran, A. Offenberger, D. Pennington,
M. Perry, T. Phillips, C. Sangster, M. Tabak, G. Tietbohl,
M. Tsukamoto, K. Wharton, S. Wilks

This paper was prepared for submittal to the
39th Annual Meeting of the American Physical Society
Division of Plasma Physics
Pittsburgh, PA
November 17-21, 1997

December 1, 1997



This is a preprint of a paper intended for publication in a journal or proceedings. Since changes may be made before publication, this preprint is made available with the understanding that it will not be cited or reproduced without the permission of the author.

DISCLAIMER

This document was prepared as an account of work sponsored by an agency of the United States Government. Neither the United States Government nor the University of California nor any of their employees, makes any warranty, express or implied, or assumes any legal liability or responsibility for the accuracy, completeness, or usefulness of any information, apparatus, product, or process disclosed, or represents that its use would not infringe privately owned rights. Reference herein to any specific commercial product, process, or service by trade name, trademark, manufacturer, or otherwise, does not necessarily constitute or imply its endorsement, recommendation, or favoring by the United States Government or the University of California. The views and opinions of authors expressed herein do not necessarily state or reflect those of the United States Government or the University of California, and shall not be used for advertising or product endorsement purposes.

Hot electron production and heating by hot electrons in fast ignitor research

M. H. Key, K. Estabrook, B. Hammel, S. Hatchett, D. Hinkel, J. Kilkenny, J. Koch, W. Kruer, B. Langdon, B. Lasinski, R. Lee, B. MacGowan, J. Moody, M. Moran, A. Offenberger, D. Pennington, M. Perry, T. Phillips, C. Sangster, M. Tabak, G. Tietbohl, M. Tsukamoto, K. Wharton, S. Wilks.

Lawrence Livermore National Laboratory, P.O. Box 808, L-488, Livermore CA 94550

Abstract

In an experimental study of the physics of fast ignition the characteristics of the hot electron source at laser intensities up to 10^{20} Wcm⁻² and the heating produced at depth by hot electrons have been measured. Efficient generation of hot electrons but less than the anticipated heating have been observed.

The concept of isochoric fast ignition originated by Tabak et al. ¹ is of importance through its potential to give higher inertially confined fusion (ICF) gain than isobaric central spark ignition used in the more developed indirect and direct drive schemes ² and thereby to reduce the driver efficiency required for inertial fusion energy (IFE). The physics is new and challenging involving strongly relativistic laser plasma interactions and transport of energy by MeV electrons where electrostatic potentials and self generated magnetic fields may strongly modify the transport ³. Experimental and theoretical studies aimed at assessing the feasibility of fast ignition as a new route to ICF are now being carried out at many laboratories world wide including the Lawrence Livermore National Laboratory (LLNL), where the Nova laser facility has been adapted to generate petawatt pulses using chirped pulse amplification (CPA)⁴.

Experimental Facility

Two beam lines at Nova have been adapted for CPA operation and for experiments reported here, generated typically 20J and 500J pulses respectively of duration in the range 0.4 to 20 ps (maximum power up to 1 PW). Focusing of the two beams respectively was with an off axis *f*/3 parabolic mirror of focal length 42 cm in a focal spot of 15 μ m diameter

and an axial $f/4$ parabola of focal length 170 cm in an asymmetrical spot of $40 \mu\text{m} \times 20 \mu\text{m}$. The focal spots had a speckle pattern sub structure with a broad power spectrum of intensity. Work is in progress to correct the wavefront using a deformable mirror. The 20J beam line produced a power weighted average intensity on target in 0.45 ps pulses estimated at $2 \times 10^{19} \text{ Wcm}^{-2}$. The 500J, beam line produced 10^{20} Wcm^{-2} in 1 PW, 0.45 ps pulses. A thick glass plate debris shield protected the parabola in the 500J beam line for longer pulse operation down to 5 ps. Non linear effects precluded the use of the debris shield for 1PW shots and here a plasma mirror was used to reverse the beam direction thus projecting ablated target debris away from the un-protected parabola. The off axis parabola was used with a thin debris shield for all pulse lengths in the 20 J experiments. Targets in these experiments were exposed to ASE and leakage prepulses before the main pulse. ASE in a typically 3 ns period before the pulse varied in experiments reported here from 2×10^{-5} to 2×10^{-4} of the main pulse energy. The energy of leakage pulses ranged from 10^{-4} to 10^{-2} of the main pulse, occurring 2 ns or 4 ns before the main pulse but could be made as low as 10^{-6} with precise adjustment of Pockels cell gates.

The hot electron source

K α spectroscopy

A central theme of the experimental work has been the characterization of the hot electron source produced at a solid target. Electrons directed into the target are required in fast ignition to heat compressed (200 to 600 g/cc) thermonuclear fuel to ignition conditions (15 keV and density radius product ρr of 0.5 gcm^{-2}). Electrons of about 1 MeV energy have the necessary range.

Extensive experiments were carried out with the 20J, 0.4 ps beam at 25 degree P polarized incidence on flat layered targets. A Mo fluor layer 50 micron thick was sandwiched

between a front layer of variable material and thickness and a 1 mm thick polymer back layer. Electrons from the focal spot on the front layer penetrated into the target and induced $K\alpha$ fluorescence in the Mo which was recorded via the back of the target by a CCD camera operating as a proportional counter at signal levels giving single photon detection in each pixel. The X-ray spectrum in the vicinity of the 17.5 keV Mo $K\alpha$ fluorescence was recorded as a spectrum of counts from the CCD pixels and showed the $K\alpha$ line with a background continuum. Subtraction of the continuum gave the $K\alpha$ yield. The detector was calibrated absolutely with a 22 keV, Cd^{109} gamma radiation source.

Data were recorded for CH, Al and Cu front layers of mass per unit area up to 0.5 gcm^{-2} , the penetration depth needed for fast ignition. The results⁵ are shown in figures 1 and 2 where the depth at which the fluor layer is located is specified in units of mass per unit area because the range of an electron of a given energy is determined principally by the mass per unit area irrespective of the material. The most obvious features are the decrease in $K\alpha$ yield with increasing depth in all cases and the decrease at a fixed depth as the material is changed from Cu to Al to CH. The electrons are clearly less able to penetrate the CH target. There is a smaller reduction in penetration changing from Cu to Al.

To interpret these experiments we used two codes ITS and Lasnex. The first is a 3D Monte Carlo electron photon transport model describing scattering, energy loss and $K\alpha$ and Bremsstrahlung emission by electrons in cold matter with no self consistent potentials or magnetic fields or heating effects. The source of electrons was specified as a relativistic Maxwellian of variable mean energy with either a 90 degree or a 30 degree cone half angle. The second is plasma code Lasnex, which was run in 1D with hydro - effects switched off to describe how hot electrons created with a Maxwellian energy spectrum in a spherical

region of diameter equal to the focal spot diameter, diffuse and heat up the surrounding initially cold matter. The model computes the changing temperature and resistivity of the plasma, energy loss and heating from electron collisions, electrostatic potential, return current and ohmic heating. The 1D spherical geometry is only a rough approximation to the experiment and the Lasnex results are not therefore suitable for quantitative comparison with experiments. Potentials computed with Lasnex were comparable to the mean energy of the hot electrons only close to the focal spot and at early times. The potential well rapidly increased in radius and decreased in amplitude and was of negligible significance over most of the distance traversed by the electrons in diffusing to the fluor layer. The computed behavior for Cu, Al and CH targets was similar but the modelling of CH targets was more inaccurate as the high resistivity of cold CH was seriously underestimated by the plasma model. Ohmic $j \cdot E$ heating within the potential well was predicted to be significant accounting for example for 38% of the absorbed laser energy in Cu targets.

Based on the Lasnex modelling, use of the ITS code to model the $K\alpha$ data for Cu and Al targets was an approximation which was expected to be valid over most of the path traversed by the electrons. The code was run for a relativistic Maxwellian electron energy distribution function which was found to give a good fit to PIC code modeling⁶. The ITS model showed that typically 90% of the excitation of $K\alpha$ fluorescence was by electron collisions and 10% by the Bremsstrahlung radiation from the hot electrons. Fitting the slope of the fall off in $K\alpha$ yield with depth gave the mean energy $\langle E \rangle$ or temperature kT of the hot electrons. Fitting the absolute yield gave a conversion efficiency which was a weak function of the angular distribution of the source electrons. For Cu targets $\langle E \rangle = 0.64 \pm 0.2$ MeV and a conversion efficiency of 28% were obtained assuming a 90 degree cone half angle. The corresponding figures for a 30 degree half angle were a lower efficiency of 21% at the same mean energy. The data for Al had less scatter and assuming a 90 degree cone

half angle, were fitted with $\langle E \rangle = 330 \pm 120$ keV and an efficiency of 31%, the latter only marginally different from the Cu result within the errors. The estimated conversion efficiency is a lower bound since the $K\alpha$ measurement is not sensitive to the energy loss of the electrons to the induced potential which is recovered as ohmic $j \cdot E$ heating. An estimate of the necessary scale up in conversion efficiency is given by the ratio $(E_o + E_c)/E_c$ for the ohmic 'o' and collisionally deposited 'c' energies. For Cu this factor would give a 1.6 fold efficiency increase if the 1D model were exact. 2D modelling is needed however to give a quantitatively useful scaling factor.

The CH data are radically different and show a strong reduction of electron penetration. We tentatively attribute this to potentials generated by the electron flow in the high resistivity of cold CH which is not well modeled in Lasnex.

The discussion so far neglects magnetic fields which may modify the electron transport. For instance we estimate that the hot electron current would be 1000 times the Alfvén current if not neutralised by a cold electron return current. A reduction of electron penetration by magnetic fields would lead to a further underestimate of the conversion efficiency and/or mean energy. Our estimates should for this reason also be regarded as a lower bound.

We quote mean energy (640 keV for Cu) in preference to the temperature of the electrons for the following reasons. The temperature of a fully relativistic Maxwellian has a mean energy of $3kT$ whereas for a non relativistic Maxwellian the mean energy is $3/2 kT$. Classical Maxwellian or simple exponential forms having the same mean energy (and similar half width) but different temperatures gave essentially the same ITS model predictions for $K\alpha$ yield. Mean energy therefore seems to be invariant in the fits. PIC modeling ⁶ gives a mean energy of 690 keV at $1.2 \cdot 10^{19}$ Wcm⁻². Scaling in proportion to the relativistic ponderomotive potential (RPP) suggests that $\langle E \rangle$ given by PIC modelling would be 960

keV at $2 \times 10^{19} \text{ Wcm}^{-2}$. This is close to the 930 keV RPP at $2 \times 10^{19} \text{ Wcm}^{-2}$. The 640 keV experimental value is therefore about 70% of the RPP.

Work elsewhere has determined the temperature of the hot electrons over a range of intensity \times (wavelength)² up to mid $10^{18} \text{ Wcm}^{-2} \mu\text{m}^2$ giving scaling⁷ proportional to (intensity)^{0.3} which extrapolate to $kT = 450 \text{ keV}$ at $2 \times 10^{19} \text{ Wcm}^{-2}$. The temperature associated with our fitted $\langle E \rangle = 0.64 \text{ MeV}$ is 0.3 keV. Our lower bound measurement is therefore lower (70%) relative to other temperature measurements.

We expect experimental results in general to be significantly influenced by the form of the power spectrum of intensity on the target which for typically many times diffraction limited beams we believe is broad and similar to that in a classical speckle pattern. Relativistic self focusing in preformed plasma⁸ may further broaden the spectrum of intensity. The fraction of the power at the quoted intensity is difficult to determine in practice and differences between experiments may arise from this source.

A new but limited set of data was obtained recently with the high energy beam line. Al targets irradiated by 5 ps, 300 J pulses at 10^{19} Wcm^{-2} gave results which although scattered, were roughly fitted by the same mean energy as the results from 20 J, 0.4 ps ($2 \times 10^{19} \text{ Wcm}^{-2}$) shots, but with a reduced 10 to 15% conversion efficiency. For longer pulses at lower intensity (20 ps, 200 to 400 J pulses at $2 \times 10^{18} \text{ Wcm}^{-2}$) there was also no apparent change of mean energy but a further reduction of conversion fraction to 5 to 10%. These results show an intensity dependence of the conversion fraction if analyzed assuming a constant mean energy of 330 keV as shown in figure 3. Our preliminary interpretation of this behavior is that it is attributable to a multi-temperature 'hot tail' form of the electron energy distribution which is also evidenced in hard X-ray Bremsstrahlung spectra discussed below. The low intensity long pulse shots produce an electron distribution in which only the hot tail penetrates to the depth of the $K\alpha$ measurements

whereas in the case of the high intensity data the bulk of the electrons can penetrate to that depth. The apparent mean energy for the low intensity shots is therefore associated with the hot tail and we expect that the bulk of the electrons have a lower mean energy.

Bremmstrahlung emission

Bremsstrahlung emission by the hot electrons gives useful additional information. In the case of thick high Z targets, Bremsstrahlung from the target itself dominates over that from the target chamber walls. Data of this type were obtained at normal incidence on Au targets with both 5 ps and 0.5 ps pulses from the high energy beam line.

Using the PW, 0.5 ps beam reflected by a plasma mirror, the typical energy on target assuming 70% plasma mirror reflectivity, was 330 J and the power weighted mean intensity was up to 10^{20} Wcm⁻². The forward directed X-ray Bremsstrahlung spectrum from 1 mm thick Au targets was measured at 45 degrees from the laser axis using Li₂B₄O₇ and CaSO₄ TLD detectors recording via 5 different absorber filters the most absorbing of which was 3 cm of Ta. The detectors were absolutely calibrated using a Co⁶⁰ 1.33 and 1.173 MeV gamma source. The X-ray spectrum was inferred iteratively from the TLD data using a Monte Carlo model to compute the TLD signals from the assumed X-ray spectrum. This is a well established unfolding technique and it gave results for the absolute spectral intensity shown in figure 4. Similar data were recorded with 350 J, 5 ps pulses in the debris shield configuration as also illustrated in figure 4 and these showed as expected reduced spectral brightness at high photon energy.

In such a spectrum a Maxwellian electron energy distribution gives an $\exp(-hv/kT)$ spectral shape and the slope of a logarithmic plot gives the temperature of the electrons. As has often been seen in laser plasma studies, the slope of the spectrum in figure 4 changes significantly with increasing photon energy to indicate apparently higher temperature at

higher photon energies. This shows that the electrons do not have a simple Maxwellian energy distribution and that there is a pronounced 'hot tail' in the distribution.

The ITS code was used to model these data also, in this case computing the Bremsstrahlung rather than the $K\alpha$ yield. For the 0.5 ps data it was found that at photon energies > 1 MeV a relativistic Maxwellian of $\langle E \rangle = 6$ MeV ($kT = 2.2$ MeV) gave a reasonable fit to the measured forward directed spectrum if it contained 1.2% of the laser energy in a 30 degree cone angle. A relativistic Maxwellian of mean energy 1.5 MeV (temperature 600 keV) with 12% of the laser energy in a 30 degree cone gave a rough fit to the lower energy part of the X-ray spectrum below 1 MeV. Based on our previously discussed data the expected mean energy is 70% of the RPP at 10^{20} Wcm⁻², i.e., 2.6 MeV. The data seem to show a minor part of the electron energy spectrum with higher mean energy (6 MeV) and the majority of electrons with a lower mean of 1.5 MeV. The total energy in the electrons is more difficult to determine as it requires knowledge of the angular distribution of the X ray emission. Our data also show evidence of forward peaking of the emission as illustrated in figure 5 which plots data from Si diodes filtered to record a spectrum of mean energy 1MeV, but we do not have sufficiently extensive data for an angular integration. These results may simply indicate a wide range in the power spectrum of intensity at the critical density, enhanced by relativistic self focusing in prepulse formed sub critical density plasma or the hot tail may be specifically associated with electron acceleration in relativistically self focused filaments at sub critical density. Further work is needed to distinguish between these two possibilities.

Electron energy spectra

Corroboration of the hot tail in the electron energy spectrum was obtained from magnetic spectrometer measurements of electrons escaping from the target. The detector was nuclear emulsion recording the tracks of individual electrons. Two spectrometers were placed at 30 degrees and 95 degrees from the laser axis producing spectra from 1 mm thick Au targets shown in figure 6. The recorded electrons had a mean energy of 7 MeV with maximum energies up to 100 MeV being recorded. The integrated energy per steradian in the forward direction was about 1% of the laser energy, reflecting significant electron energy loss escaping from the potential well together with collisional energy loss in penetrating through the target.

Photo neutrons and nuclear activation

The highest energy photons in the Bremsstrahlung spectrum induce nuclear processes which give further quantitative evidence of the spectral brightness at photon energy in the region of 20 MeV. Nuclei generally exhibit a giant resonance for photo neutron emission and the magnitude of the cross section and its energy threshold vary with atomic number, but in general the resonance has a band width which is narrow enough to give an estimate of the spectral intensity at its peak from the yield of photo neutrons⁹. This yield is most easily deduced by measuring the characteristic gamma emission of the activated nuclei which result from the emission of photo neutrons, though it can also be determined from activation and gamma emission consequent on capture of the photo neutron by a high Z nucleus or direct detection of the neutron. Data were obtained with massive high Z targets including for example a 1 cm wide 1 cm long solid target with layers of Au, Ni, In and Al which was irradiated with a 5 ps 300 J pulse at 10^{19} Wcm⁻². The yield of photo neutrons in Ni⁵⁸ was inferred to be $9 \cdot 10^5$ from measurement of 0.5 and 14 MeV gamma decays of the excited Ni⁵⁷ nucleus produced by photo-neutron emission. A similar result from 300 J irradiation of an Au /Cu target gave $4.5 \cdot 10^7$ photo-neutrons from Cu. Assuming a slowly

varying spectral intensity in the vicinity of the giant resonance these data give the spectral intensity at 18.5 MeV and 21.8 MeV respectively which are plotted in figure 4. There is fair agreement with extrapolation of the Bremsstrahlung spectra for both the 5 ps and 0.5 ps cases confirming the hot tail feature in both those spectra.

In summary our observations of hot electron production have shown 28% lower bound conversion to forward directed electrons of 640 keV mean energy close to the 1 MeV envisaged for fast ignition using intensity $2 \times 10^{19} \text{ Wcm}^{-2}$ and also higher electron energies at higher intensities. This is encouraging particularly when there is evidence of substantial forward peaking of the angular distribution.

Heating

The second main goal of our research is to measure heating at depth due to the hot electrons. The fast ignitor scheme assumes channel formation at subcritical density and hole boring at super-critical density giving penetration of the laser light to within about two focal spot diameters from the dense fuel. Over a range of this order it is necessary to have minimal lateral spreading of the electron flow and to produce intense heating. Accordingly we looked initially for thermal x-ray and thermonuclear neutrons from indicator layers buried at depths up to 50 micron in cold layered solid targets with minimum preformed plasma.

Our modelling base for this work was the 1D Lasnex model discussed previously which predicted heating solid matter at depth up to 20 micron to temperature of the order of 1 keV using 20 ps pulses to generate electrons of shorter range and therefore greater local heating effect.

X-ray spectroscopy

As an initial test we recorded streak time resolved X-ray spectra from 1 micron thick layers of Al with a CH over-layer of variable thickness using a flat KAP crystal spectrometer.¹⁰ The targets were irradiated with 20 ps 20 J pulses focused to a 15 micron focal spot. The results showed resonance spectral lines of hydrogenic and He-like Al with strong spectral broadening. Fitting computed spectra suggested density of 0.8 to 1.2 10^{23} electrons/cc and temperature up to 300 eV to 600 eV for 5 micron over-layer thickness. 2D Lasnex modelling shows that ablative modification of the over-layers was not negligible in this work, where the ASE prepulse was estimated at 25 mJ and a similar energy was present in a leakage pulse 4 ns before the main pulse. The fact that the density deduced from the line broadening with the 5 micron over-layer was less than solid density is probably attributable to prepulse effects.

DD nuclear fusion

An alternative potentially more sensitive measure of the heating of solid matter to >1 keV temperature is DD fusion in solid CD₂. Experiments were therefore conducted with targets incorporating CD₂ layers. Scintillator photo-multiplier neutron detectors were set up at a variety of angles and distances. Maximum sensitivity and high time of flight resolution was afforded by a specialized detector Lansa comprised of a 960 element array of photo-multiplier /scintillator detectors, the whole array being screened by 15 cm of lead shot. The Lansa array was located at 21 m from the target an angle of 260 degrees to the laser axis. Its signals were converted electronically to a digital form giving the time above a pre defined threshold signal on each channel. The other neutron detectors were single scintillator photo-multiplier units with analog recording on fast oscilloscopes.

Targets were irradiated with 20 ps and 5 ps pulses, the lower electron energy being predicted to maximize the heating close to the focal spot. The experimental data revealed

features attributable to the hot tail of the electron velocity distribution. Firstly strong signals were detected by Lansa from thin (100 micron) CH targets with no CD₂. The neutron energy spectrum deduced from the timing of the pulses at the detectors was broad, from as high as 10 MeV with the signal level rising continuously to energies below 1MeV, the limit of the range of measurement. This continuum in the time of flight spectra we attribute to γn photo neutron production in the walls of the target chamber. Adding a 10 micron thick layer of CD₂ on the surface of the target and placing a 100 micron thick disc of solid CD₂ normal to the surface to intercept 1 sterad of the ion emission from the target, gave a measure of DD fusion due to three causes - fast ions striking the CD₂ block, fast ions driven into the target by light pressure and thermal fusion due to heating by electrons. The DD fusion signature was a relatively weak feature on top of the continuum in the time of flight spectrum. The DD yield was $1.7 \cdot 10^6$ and was seen to be about 10x broader than the instrumental width for circa 1keV thermal fusion. It was approximately centered at 2.7 MeV suggesting that the dominant beam target interaction was from ions directed away from the target.

It was not possible to unambiguously detect thermal fusion but a variety of targets incorporating CD₂ layers were irradiated with both 20 ps and 5 ps pulses and neutron emission in broad energy bands was seen with both Lansa and with the simpler scintillator detectors. An upper bound figure for thermal fusion events from the Lansa data from a 10 micron CD₂ layer buried below 0.5 micron of Cu and irradiated with 400J in 20 ps was determined to be $3 \cdot 10^4$ from the data shown in figure 7. Lasnex simulations of a 10 micron CD₂ layer heated to variable initial temperature during the laser pulse with cooling by conduction and hydrodynamic expansion, gave a scaling of neutron yield with temperature from which the upper bound on the CD₂ temperature in the experiments was estimated at 800 eV.

The expected heating from the 1D Lasnex calculations was greater, temperatures over 1 keV being predicted which should have shown a thermal DD fusion yield of more than 10^5 . The apparent failure to heat as efficiently as predicted may be attributable to limitations of the Lasnex 1D model but more likely is traceable to the high prepulse level in these experiments which created a considerable plasma atmosphere through which the heating beam had to penetrate in order to reach the target. Self focusing and beam spraying in the pre-plasma could significantly increase the area of electron energy deposition in the buried layer of CD_2 and reduce the heating. Similarly failure to penetrate significantly beyond the critical density in the preformed plasma could put the source of hot electrons at a significant distance from the CD_2 layer.

Preformed plasma

The capacity of an intense beam to penetrate a pre plasma was studied by irradiating thin CH targets with 20 J pulse of both 0.5 ps and 20 ps duration. Optical probing interferometry across the target surface at the second harmonic with a short pulse derived by beam splitting from the main pulse, showed details of the pre-plasma formation as indicated in figure 8. These experiments demonstrated that 20 J, 0.5 ps pulses did not penetrate through foils of initial thickness above 1.7 micron. while 20J, 20 ps pulses penetrated up to 2 thick micron foils. There was clearly prepulse modification of the foils but the data suggest that $> 10^{-4}$ gcm⁻² of preformed plasma at supercritical density presents a significant barrier capable of preventing hole boring by a short duration 20 J pulse, underlining the need to avoid significant pre-plasma formation in order to optimize heating.

Conclusions

Initial studies with the Nova facility have shown efficient generation of electrons in a forward collimated flow and of circa 1 MeV energy of interest for fast ignition. Study of heating by the electrons has suggested a need to minimize pre-plasma production in order to optimize heating which so far has been limited to less than 1 keV and is below expectations from 1D modelling.

Acknowledgments

We are grateful for the support of the Nova operations and engineering teams. Work performed under the auspices of the US Department of Energy by the Lawrence Livermore National Laboratory under Contract No. W-7405-ENG-48.

References

-
- ¹ M Tabak J Hammer M E Glinsky W L Kruer S C Wilks J Woodworth E M Campbell M D Perry Phys Plasmas, 1, 1626, (1994)
 - ² Lindl, J. D., Laser Interaction and Related Plasma Phenomena, AIP Conf. Proc. 318 , p. 635, (1993).
 - ³ A Pukhov , J Meyer ter veht Phys Rev. Lett. 79, 2686 (1997)
 - ⁴ M. D. Perry, Science & Technology Review page 4, December 1996.
 - ⁵ K B Wharton C Brown B A Hammel S Hatchett M Key J Koch J Moody A Offenberger M Perry M Tabak S Wilks V Yanovsky Bul Am Phys Soc 42 1969 (1997)
 - ⁶ S C Wilks W L Kruer M Tabak A B Langdon Phys Rev Lett. 69 1383 (1992)
 - ⁷ P Norreys private communication
 - ⁸ A Pukhov , J Meyer ter veht Phys Rev. Lett. 76, 3975(1996)
 - ⁹ B L Berman . Atomic data and Nucl. data tables 15, 319 - 390 (1975).
 - ¹⁰ J. A. Koch, C. A. Back, C. Brown, K. Estabrook, B. A. Hammel, S. P. Hatchett, M. H. Key, J. D. Kilkenny, O. L. Landen, R. W. Lee, J. D. Moody, A. A. Offenberger, D. Pennington, M. D. Perry, M. Tabak, V. Yanovsky, R. J. Wallace, K. B. Wharton and S. C. Wilks, Lasers and particle beams (in press)

Figures

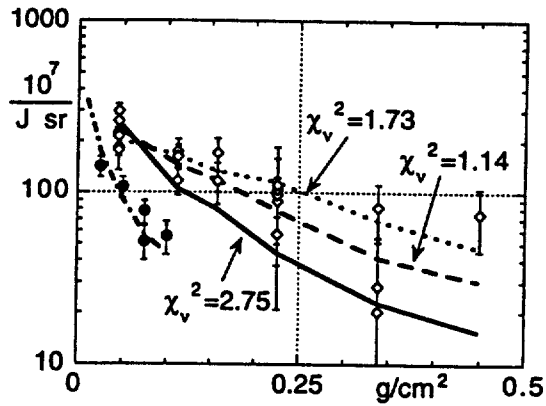


Figure 1. K_{α} signal in units of 10^7 x-rays per incident Joule per steradian, plotted against mass per unit area of the front layer of the target. The solid circles are data from CH front-layer targets, empty diamonds are data from Cu targets, both at $2 \cdot 10^{19} \text{ W cm}^{-2}$. The solid line is an ITS fit in Cu with $E_0=330\text{keV}$ and conversion efficiency $E_{\text{elec}}/E_{\text{laser}}=30\%$. The dashed line is $E_0=640\text{keV}$ and $E_{\text{elec}}/E_{\text{laser}}=29\%$. The dotted line is $E_0=1040\text{keV}$ and $E_{\text{elec}}/E_{\text{laser}}=31\%$. The dash-dot line is an ITS fit in CH for $E_0=120\text{keV}$ and $E_{\text{elec}}/E_{\text{laser}}=29\%$.

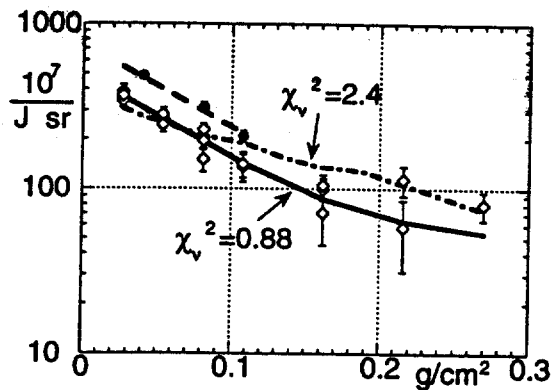


Figure 2. K_{α} signal from the Al targets, in units of 10^7 x-rays per incident Joule per steradian, plotted against mass per unit area of the Aluminum front layer of the target. The solid circles are experimental data at intensities of $4 \cdot 10^{19} \text{ W cm}^{-2}$, empty diamonds are data at $2 \cdot 10^{19} \text{ W cm}^{-2}$. The solid line is an ITS fit with $E_0=330\text{keV}$ and conversion efficiency $E_{\text{elec}}/E_{\text{laser}}=31\%$. The dash-dot line is $E_0=640\text{keV}$ and $E_{\text{elec}}/E_{\text{laser}}=30\%$. The dashed line is $E_0=330\text{keV}$ and $E_{\text{elec}}/E_{\text{laser}}=47\%$.

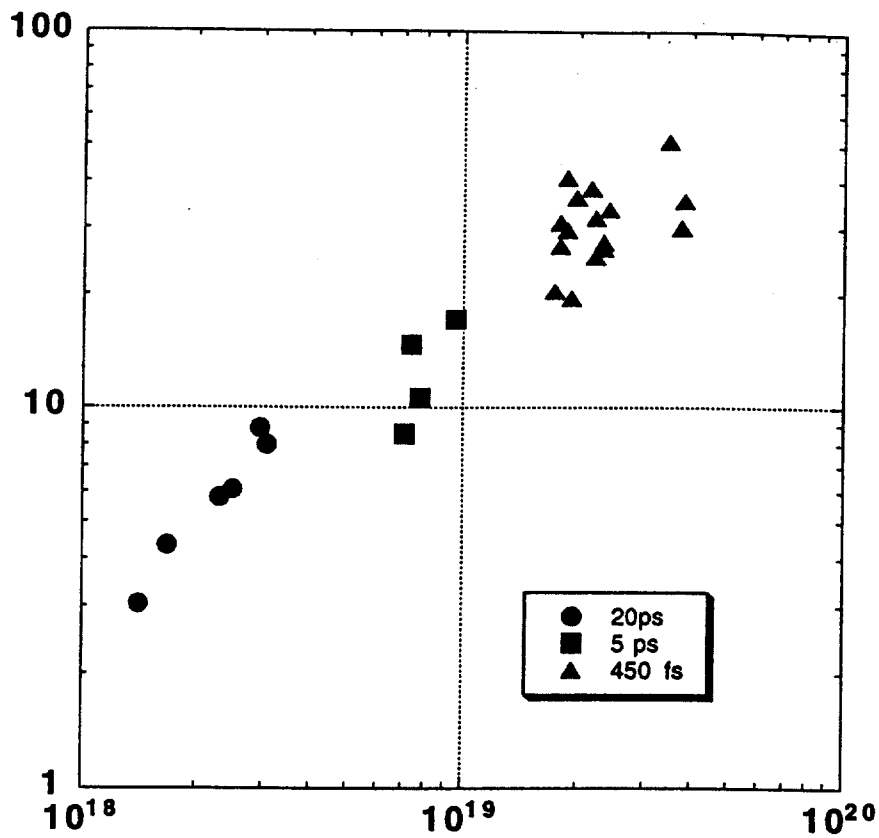


Figure 3. Ordinate efficiency $E_{electron}/E_{laser}$, abscissa intensity on target $W\ cm^{-2}$ 20 Ps and 5 ps data are for high energy, 200 to 400 J and 450 fs data are for 15 to 20 J

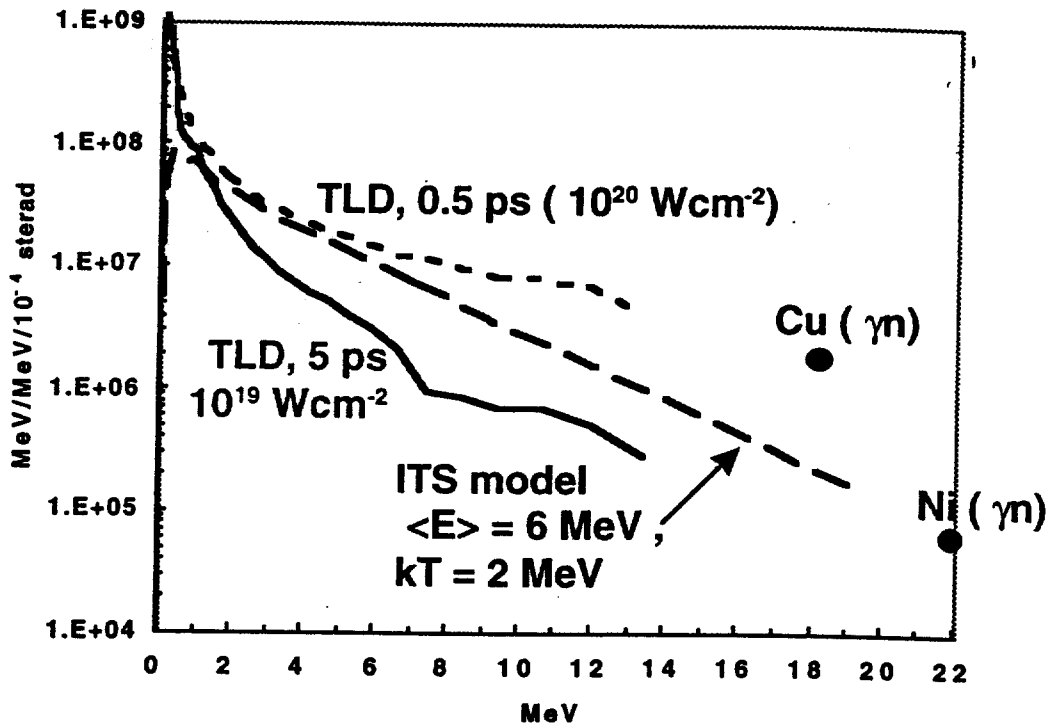


Figure 4 Ordinate ; X-ray intensity MeV/MeV in 10^{-4} sterad . Abscissa ; photon energy
Spectral data from TLD measurements as labeled . ITS model data as labeled and
activation data as labeled

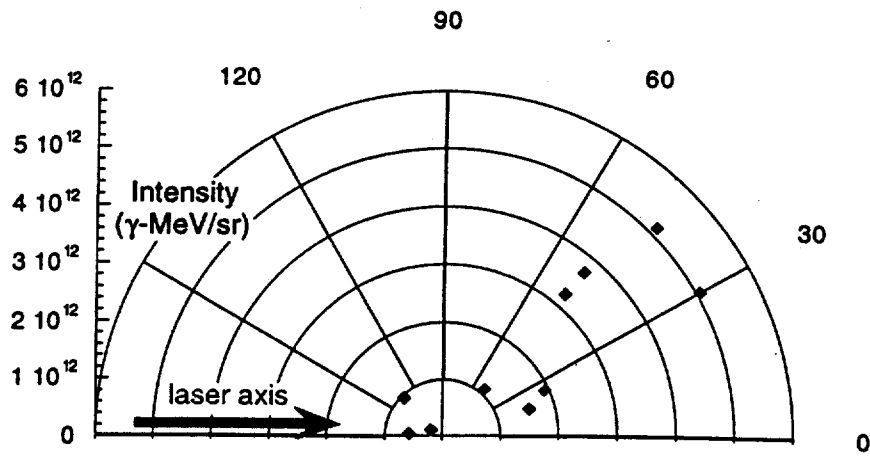


Figure 5 Polar plot of X-ray intensity in MeV/sterad for 0.5 ps , squares , and 5 ps pulse length diamonds for 300 J pulse incident on thick Au targets

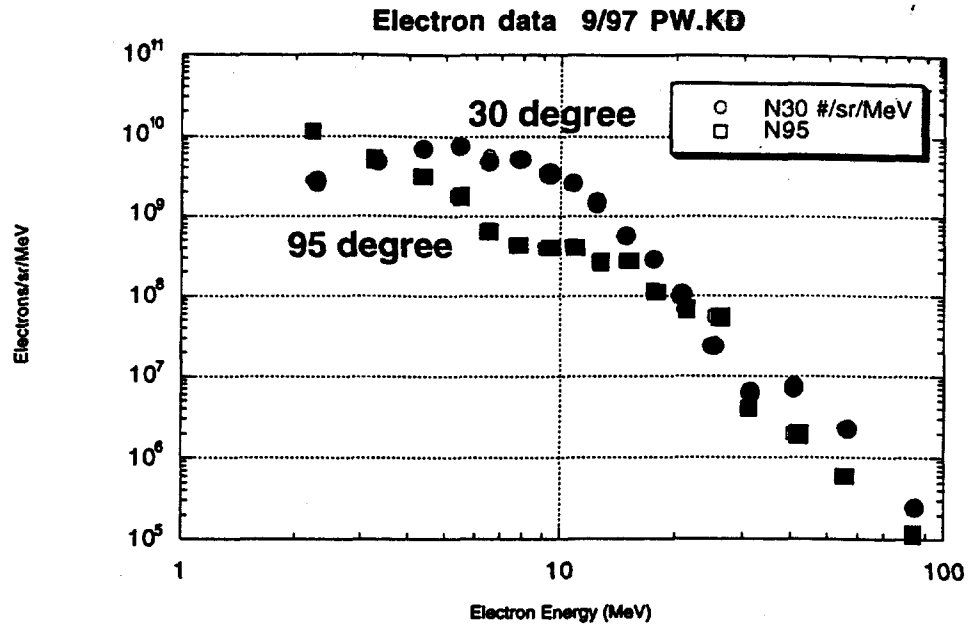


Figure 6. Ordinate ; electrons /sterad/MeV . Abscissa ; electron energy MeV . Data at 30 degrees , filled circles and 90 degrees , filled squares , to the laser axis

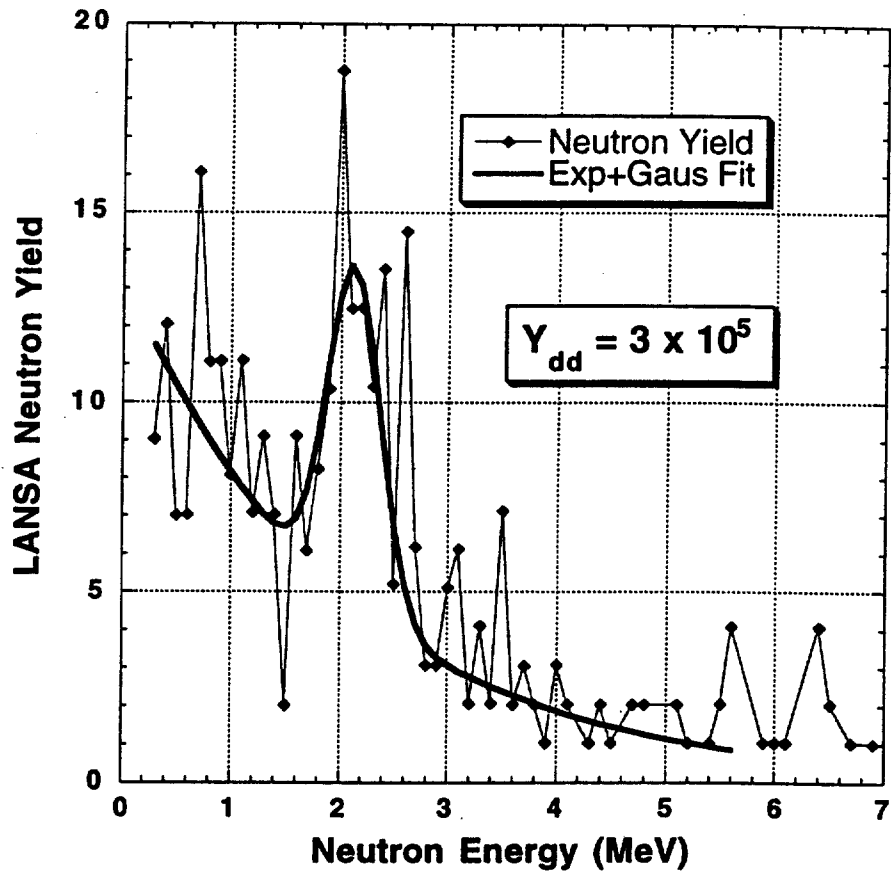
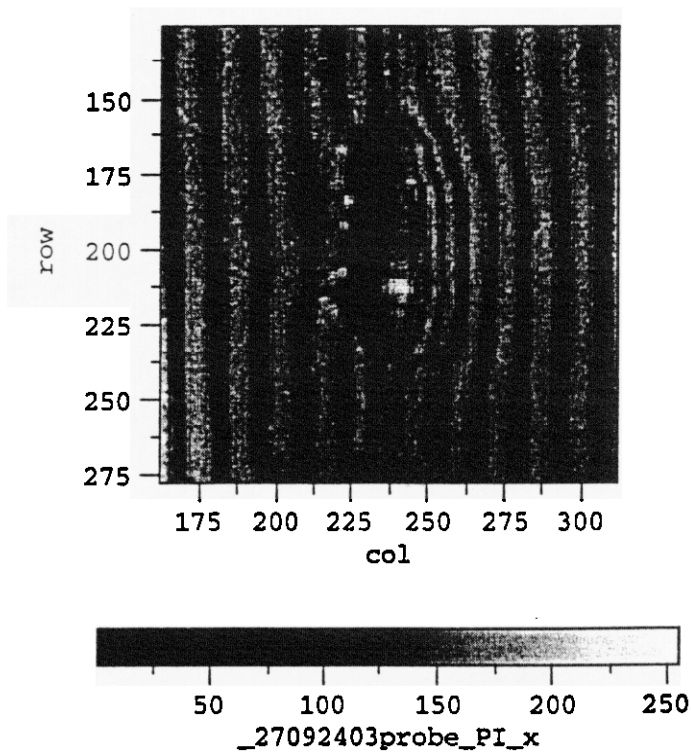


Figure 7 Ordinate; neutron yield in arbitrary units . Abscissa ; neutron energy . The DD fusion feature is seen above a continuum due to photo - neutron emission at the target chamber walls



150 micron

Figure 8 Interferogram recorded with a sub-picosecond pulse of second harmonic light 1ps before the main pulse on a 2 micron CH target showing plasma formation due to ASE and leakage pulses .

Technical Information Department • Lawrence Livermore National Laboratory
University of California • Livermore, California 94551

